PHOTORESIST DISSOLUTION MECHANISM STUDIES

by

Andrew M. Zenk

Memorandum No. UCB/ERL M96/30

28 May 1996

PHOTORESIST DISSOLUTION MECHANISM STUDIES

by

Andrew M. Zenk

Memorandum No. UCB/ERL M96/30

28 May 1996

ELECTRONICS RESEARCH LABORATORY

College of Engineering
University of California, Berkeley
94720

PHOTORESIST DISSOLUTION MECHANISM STUDIES

by

Andrew M. Zenk

Memorandum No. UCB/ERL M96/30

28 May 1996

ELECTRONICS RESEARCH LABORATORY

College of Engineering
University of California, Berkeley
94720

Photoresist Dissolution Mechanism Studies

Andrew M. Zenk

M. S. Project
Spring 1995

Professor A. R. Neureuther
Department of Electrical Engineering and Computer Sciences
University of California at Berkeley

Abstract

An introduction to photoresist materials is presented, followed by a discussion of current modelling practices, focusing on dissolution models. The need for physical understanding of dissolution mechanisms is motivated. The results of experimental work and simulations on four negative chemically-amplified photoresists with varied crosslinker structure are detailed, revealing some drawbacks in current kinetic models and showing that crosslinker structure has little overall effect on dissolution characteristics. Recent advances and current research in describing polymer dissolution mechanisms are discussed, and a simple simulation program of chain-scission is applied to find the molecular weight distribution of PMMA after electron-beam exposure. Finally, directions for future research are presented, suggesting the design of some experiments and future simulation programs.

Table of Contents

1.0 Introduction

The lithographic process was developed initially for use in the offset printing industry, in which writings and designs are defined on a master metal plate, and this plate is then used to print numerous paper copies of the writing. Writings are generated on the plate by applying a photographic film to the plate surface, exposing it through a mask with the written patterns, removing the exposed film with a development step, and applying an etchant to define the writings in the surface of the plate. Etching is blocked by the film everywhere except where the film has been removed, and a permanent copy of the writings is retained in the plate surface. The photographic films employed by this process are traditionally photosensitive organic materials dubbed "photoresists", from "photo" for photosensitive, and "resist" for the film's resistance to etchant, thus defining the two basic properties the film must have.

The semiconductor industry has borrowed this process to define circuit patterns on the surface of a silicon wafer. The incredibly small size of integrated-circuit (IC) dimensions places very high demands on the resolution of lithographic pattern-transfer systems, including the photoresist image recording material (or simply "resist"). In order to be effectively resistant to other IC manufacturing processes such as ion implantation, features in the photoresist film must be uniform in thickness and have nearly vertical profiles. From a manufacturing standpoint, resolution and etch resistance are not the only important resist qualities - it must also be reliable, safe, and require minimal energy doses to become exposed.

There are several different types of materials that are useful as resists. These can be grouped into positive-tone resists, whose solubility increases with exposure, and negative-tone resists, whose solubility decreases with exposure. These groups can be further divided into one-component, two-component, and other systems. One-component resists are simply a photosensitive polymer that absorbs exposure energy, which causes chain scission (positive) or crosslinking (negative). Two-component resists consist of a photo-insensitive polymer and a photoactive compound (PAC) that undergoes a structural change upon irradiation, which affects a change in solubility of the polymer. Other more complicated materials have also been developed, including the negative three-component resists which will be discussed in chapter 3. Negative three-component resists contain a photo-insensitive polymer, a photoactive compound, and a crosslinker molecule. In these resists the PAC serves to generate an acid (thus the PAC is more accurately called a photoacid generator, or PAG), which subsequently reactes with the crosslinker molecule to form a crosslinked, insoluble polymer. Some positive three component resists have been made by modifying two-component systems. A great advantage of some three-component resists is that the acid can be regenerated, thereby achieving a quantum efficiency greater than one ("chemical amplification"). This can be very important at higher frequencies such as ultraviolet, where low-energy sources such as the mercury arc lamp are typically used, because it greatly reduces the amount of energy necessary to change the solubility of the resist.

The resist system currently favored by industry is the novolac/DNQ combination developed by Oskar Süss of Kalle Corporation in Germany during the 1930s and 1940s.[1] This is a two-component positive system containing a novolac polymer and a diazonaphthoquinone (DNQ) PAC. Much is yet to be understood about these resists, and they are one of the main topics of chapter 4.

The processing of photoresists involves four essential steps. First, a solution of resist and organic solvent must be applied to a silicon wafer, usually by a spin-on technique. Second, the solvent must be evaporated to leave a solid resist film. This is accomplished by heating the wafer and boiling the solvent, in what is known as the "post-applied" or "pre-exposure" bake. Third, the resist is selectively exposed through a mask (containing the circuit information). In most resists, the chemistry that leads to developer selectivity occurs in this step. The fourth step is development, during which an etchant is applied to the wafer, removing the exposed (in a positive-tone resist) or unexposed (in a negative-tone resist) areas of the resist film. The etchant is usually an organic solvent or an aqueous base ("wet" development, or dissolution) depending on the structure of the polymer, but as feature profiles become increasingly critical, an emphasis is being placed on using plasmas as etchants ("dry" development) to achieve the necessary etching anisotropy. Preparing films for dry development usually requires several extra processing steps. In most three-component resists, an additional step of heating the wafer prior to development and after exposure (a "post-exposure" bake) is necessary to drive the acid-catalyzed reaction.

As the complexity of photoresist materials increases, so must modelling capabilities. Current IC process simulators such as SAMPLE have fairly good models for resist exposure (and post-exposure bake if necessary), but dissolution models are mostly empirically-based. Quantitative understanding of resist dissolution mechanisms has (and still is) slow in forthcoming, but such an understanding is precisely what is needed to support the overall optimization and design of resist materials in the context of the complex trade-offs that must be made in developing advanced technologies.

The process of establishing mechanism-based models can be greatly accelerated through simulation and the examination of materials with systematic variations in their synthesis. This paper presents some of each. After a brief discussion of current dissolution models, the results of experiments on a series of analogous negative three-component resists in which the crosslinker molecular structure was varied are presented, followed by a discussion of dissolution at a molecular level and the results of a preliminary simulation program. Some suggestions for future work are included at the end.

2.0 Dissolution Modelling Background

Several different types of models have been developed for photoresist exposure, post-exposure bake (if necessary), and dissolution. In this section a brief discussion of current dissolution models is presented, and an attempt is made to motivate the development of a molecular-level mechanistic dissolution model.

2.1 Current models

Exposure is characterized by measuring the transmittance of a photoresist film (spun on a transparent substrate) as it is exposed. The absorbance of the film decreases as the PAC absorbs energy, a process known as "bleaching" which provides a convenient measure of the concentration of exposed PAC in the resist. The ABC model devised by Dill[2] uses two differential equations to give the PAC distribution as a function of depth into the resist for a given exposure dose. This model requires three coefficients which are easily determined by the bleaching experiment.

For chemically-amplified resists, post-exposure bake has the effect of driving a reaction between the photoacid and the (acid-sensitive) material that causes a change in resist solubility. The most widely-used model for this step of the process is based on two rate equations, one which describes the reaction rate and the other which describes a rate of acid "loss", which must be included to stop the reaction.[3] These equations require two constants, which can be experimentally determined by monitoring certain infrared absorption peaks during the post-exposure bake (usually accomplished with a Fourier-transform infrared (FTIR) spectroscopy tool), and also the concentration of photoacid from the exposure model. Work is currently being done to determine how the photoacid diffuses through the resist.[4]

While models for exposure and post-exposure bake are derived from physical principles and have proven to be fairly accurate, dissolution is much more complicated. Several different models have been suggested, but to date the only ones that give reasonable simulation results are empirical curve-fits. Empirical data is often presented in the form of average dissolution rate vs. exposure energy, as shown in figure 1. Data such as this can be obtained by subjecting a number of large-area regions on a resist film to varying exposure doses, and then using laser interferometry to monitor the thickness of the film in each zone as it dissolves.

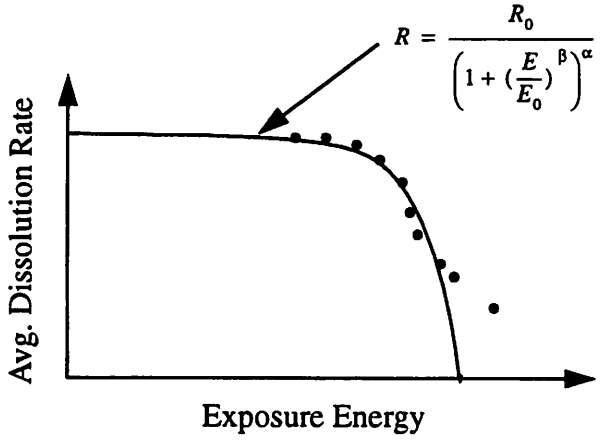

Figure 1. Typical dissolution rate vs. exposure energy curve for negative photoresists. The solid line is an example curve fit to the empirical data (the black dots). The curve-fit equation is used in simulator programs such as SAMPLE to describe negative chemically-amplified resists.[8]

The most basic dissolution models simply fit a curve to a set of data, such as that shown in figure 1. This leads to an equation relating the average resist dissolution rate to the exposure energy, ignoring all intermediate reactions or process steps. Such models have been developed for many positive and negative resists.[5, 6] Slightly more in-depth models take dissolution rate vs. exposure dose data and, along with the ABC exposure model, back out a dissolution rate vs. exposed PAC concentration curve.[2, 7-10]

While these types of empirical models are relatively easy to implement and work for specific photoresist systems that have been well characterized, they have many drawbacks. First, they provide only an average bulk dissolution rate. Most resists exhibit some type of surface inhibition effect which causes a delay in the resist response to developer chemicals,[10] and contamination of the resist by basic airborne contaminants also has an effect on surface properties.[11] Second, they don't provide any information about mechanical properties of the film, such as bridging[12] and swelling[13] in negative crosslinking resists. Third, since no insight into the resist chemistry is provided, a new model is needed for each material. In addition, the window of processing conditions over which these models are valid is generally small. It is apparent that any model to be used in the design of new complex resists must include much more information about the underlying mechanisms by which dissolution occurs.

Some attempts have been made at modelling on a more molecular level. The most prominent comes from the observation that in some resists, the dissolution rate is related to the molecular weight (presumably the number-averaged weight) of the polymer by a relation such as the following:[14]

$$Rate = \frac{\beta}{MW^{\alpha}} \qquad 2.1$$

where α and β are empirical constants. In order to use this expression for the average dissolution rate, one must also have an expression for the relationship between the polymer average molecular weight before and after exposure (and post-exposure bake if necessary). This type of expression has been developed for the simplest one-component resists, and also exists for three-component negative chemically-amplified resists.

In one-component positive resists, an exposure event causes a bond-breaking reaction to occur in the polymer, decreasing the polymer average molecular weight. A simple statistical analysis beginning with a random distribution of exposure events can be carried out to relate the pre- and post-exposure average polymer molecular weights,[12, 15] resulting in an expression such as

$$\frac{1}{M_n} = \frac{1}{M_n^0} + \left[\frac{G(s)}{100N_A}\right]D \qquad 2.2$$

where M_n is the number-averaged molecular weight after irradiation, M_n^0 is before irradiation, $G(s)$ is the number of chain scissions produced per 100 eV of absorbed energy, and D is the exposure dose. A similar expression can be derived for one-component negative resists which form crosslinking bonds upon exposure to increase the average molecular weight, but network polymers formed by these reactions have very different properties than linear polymer solids with comparable molecular weights. Thus this simple dissolution model may not be valid for crosslinking materials. Chapter 4 contains more discussion on these types of model.

A more complicated extension of equation 2.1 was developed by Ferguson[3] to describe crosslinking in a three-component negative chemically-amplified resist useful in ultraviolet lithography. In three-component resists, crosslinking is viewed as a two-step process, the first step being activation of sites on the crosslinker molecule in an acid-catalyzed reaction, and the second step being the bonding of these activated sites with nearby macromolecules to form crosslinks.

The first step is modelled by the post-exposure bake differential equations discussed previously, relating the concentration of activated crosslinking sites to the concentration of photoacid produced during exposure, assuming the quantum efficiency of the acid-catalyzed reaction is known. This leads to the following two equations describing the bake:

$$\frac{\partial C_{AS}}{\partial t} = k_1 C_{US} C_A^m \qquad 2.3$$

$$\frac{\partial C_A}{\partial t} = -k_2 C_A \qquad 2.4$$

where C_{AS} is the normalized concentration of activated crosslinking sites, $C_{US}(=1-C_{AS})$ is the concentration of unactivated sites, C_A is the concentration of photoacid, k_1 and k_2 are Arrhenius

rate coefficients, and m is a model parameter.

The second step is modelled with a statistical analysis of the crosslinking, with each crosslinking event combining two macromolecules to increase the average molecular weight of the system, which is then used in equation 2.1 to give an average dissolution rate. The resulting equation is

$$Rate = R_0 (1 - \frac{CE}{C_0})^{\alpha} \qquad 2.5$$

where R_0 is the background dissolution rate for unexposed regions and C_0 and α are curve-fit parameters. CE is the concentration of crosslinking events, with an event defined as when a crosslinking molecule bonds with two *different* macromolecules. Ferguson postulated that the number of crosslinking events is based on the number of crosslinker molecules that exist in the resist and the number of sites on each molecule that are available for crosslinking. These statistics are contained in the following two equations:

$$CE = n_m \sum_{k=2}^{n_s} (k-1) P(k) \qquad 2.6$$

$$P(k) = \binom{n_s}{k} C_{AS}^k (1 - C_{AS})^{n_s - k} \qquad 2.7$$

where n_m is the number of crosslinker molecules present, n_s is the number of available crosslinking sites per molecule, and $P(k)$ is the probability of activating k of the n_s sites.

This complicated model involves many parameters, not all of which have a physical meaning or are easily acquired. It is clear that equations 2.5, 2.6, and 2.7, and hence the average dissolution rate, are very sensitive to n_s, the number of available crosslinking sites on each crosslinker molecule. In chapter 3, several analogous resists with varying n_s are examined to see if real materials exhibit this sensitivity. It is also worth restating that the simple molecular-weight dissolution model of equation 2.1 may not be valid for network polymers formed by crosslinking.

Molecular-weight models have much the same advantages and disadvantages as the empirical curve-fit models. They still provide only an average bulk dissolution rate, and still require many experimentally-determined parameters. A further extension of equation 2.1 was developed by Scheckler, et. al,[16] to apply it on a microscopic level to individual macromolecules. In this approach, each macromolecule is represented by a sphere whose size is determined by the molecule's mass and calculated radius of gyration.[17] The packing of several spheres in a three-dimensional matrix is governed by the measured polymer density. Chain scission and crosslinking cause the cutting of one sphere into two smaller spheres or the combination of two spheres into one larger sphere, respectively. The probability that a given sphere will dissolve is proportional to the amount of surface area of that sphere exposed to developer, and inversely proportional to the size of the sphere. A computer keeps track of the location and size of each sphere, and an algorithm is then used to simulate the removal of spheres. This in effect is nearly identical to equation 2.1, with the important exception that it provides information about the resist surface as dissolution proceeds, giving a measure of the expected surface roughness of partially-developed films. However, it is not known whether a sphere is an adequate description of the macromolecular shape.

A general advantage of the molecular-weight models is that they are more physically based, and can theoretically be applied to many resist systems if valid. Of course, they only potentially apply to photoresists that undergo changes in molecular weight to differentiate between exposed and unexposed regions. Two- and three-component positive resists (and some negative resists as well) do not use molecular weight changes to achieve developer selectivity, and thus a completely different approach must be taken.

2.2 Is molecular-level modelling necessary?

As IC feature sizes shrink below 0.1-μm, new photoresist concerns arise. Issues such as surface roughness become increasingly important. In addition, lithography tools employ higher-frequency radiation to push the diffraction limit, and new resist materials must be developed that perform at these frequencies. Resists in current use are also continually being improved. Design of new photoresists, which is still very much an "ad-hoc" process, must be made more scientific. An integral part of design is accurate mechanistic models which can simulate a hypothetical material's performance.

Until recently, the roughness of photoresist film surfaces has been so small that it didn't affect the integrity of features. But roughness magnitude has the potential to become a significant fraction of the feature size,[18] leading to degraded feature quality and more error in critical circuit performance predictions. Traditionally, surface roughness has been described in terms of shot noise, attributing "bumps" and "valleys" on a resist feature's surface to statistical fluctuations in exposure.[19-21] Little agreement has been reached regarding how to characterize shot noise and what limits it imposes on the ultimate resolution of a lithography system.

As the calculated "shot noise limit" is continually surpassed, it appears that the magnitude of surface roughness in some resists is approaching molecular size.[22, 23] Thus the roughness may actually be due to a combination of shot noise and the finite macromolecular size. Some attempts have been made to relate roughness to properties of the resist polymer backbone.[16, 24] Results of this work show that polymer backbone "stiffness", average molecular weight, and polydispersity all affect the magnitude of observed roughness. A polymer molecule with less freedom to rearrange its conformation due to steric hindrances along its backbone leads to a rigid resist that exhibits large roughness. Lower molecular weight polymers exhibit small roughness, as do polymers with small polydispersity.

At this point it seems clear that better photoresist dissolution modelling techniques are necessary. Existing models are not generally applicable and have limited use in the design of new materials. Mechanistic models will hopefully excel in these areas. But in order to develop a mechanistic model, the underlying physics and chemistry must be understood. For that, it is necessary to examine photoresist dissolution on a molecular level. Once the molecular science is better understood, a macroscopic theory can be developed based on this science with direct application to mechanism-based models. This is no small task! The physics and chemistry of interactions between amorphous macromolecular solids and liquid solvents appears incredibly complicated. The following chapters describe some first steps that are being taken to get a handle on this very difficult problem.

3.0 Crosslinker Studies

The process of establishing mechanism-based models can be greatly accelerated through the examination of materials with systematic variations in their synthesis. This section presents the results of basic dissolution and imaging performance studies of a series of analogous resists with varying crosslinker molecular structure. The results are compared to those of Shipley SNR248,[25] a commercially available resist with similar structure. Ferguson's dissolution model,[3] discussed in chapter 2, is applied to test its validity.

3.1 Materials

Four experimental photoresists were supplied by Dr. J. M. J. Fréchet's resist synthesis group at Cornell University. These resists, called ML93,[26] ML239, ML240, and ML241,[27] consist of the crosslinker, poly(4-hydroxystyrene) (PHOST) polymer, and an onium salt PAG. Figure 2 describes the resist chemical composition, and also shows the structure of the crosslinking molecule in each of the resists.

From figure 2 it can be seen that three of the resist crosslinkers (ML93, ML240, and ML241) have two sites available for PHOST crosslinking. These two sites are the benzylic hydroxyls of each crosslinker molecule. The two phenolic hydroxyls of ML93 and the single phenolic group of ML240 are incorporated to enhance the solubility of the resist formulation in an aqueous base and do not participate directly in the crosslinking process. The fourth crosslinker, ML239, has four benzylic hydroxyls available for crosslinking as well as two solubilizing phenolic hydroxyls. Comparing the dissolution characteristics of these four resists should provide some insight into which properties of the crosslinker might play a role in the shape of the dissolution rate function and the resulting resist profiles, as well as being an excellent test of the Ferguson model.

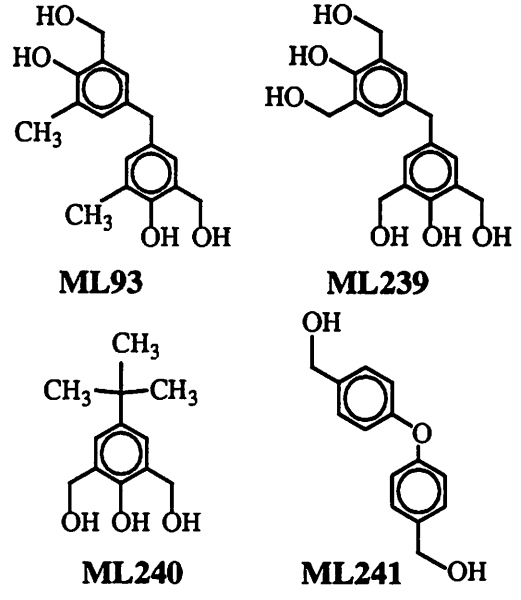

Composition:	
crosslinker	0.9 wt.%
onium salt	0.4 wt.%
poly(4-hydroxystyrene)	19.6 wt.%
diglyme	79.1 wt.%

Figure 2. Structure of the crosslinking molecule in ML93, ML239, ML240, and ML241, and the chemical composition of all four resists. These four resists are identical except for the crosslinker structure as shown.

Experiments to evaluate the performance of these resists used Shipley SNR248 as a comparison. SNR248 is known to be a production-worthy chemically-amplified resist, and thus provides a reasonable benchmark with which to measure new negative resist materials. The crosslinker in SNR248 is a melamine with six reactive hydroxymethyl groups, all theoretically available for crosslinking.[25] The polymer of SNR248 is also PHOST.

3.2 Experimental

All five resist materials were processed in the same way to facilitate comparison of results. Prior to application of the photoresist, all silicon substrates were baked for several hours in a 120°C oven and primed in a hexamethyldisilizane (HMDS) bubbler for 10 minutes to maximize adhesion. One-μm-thick photoresist films were applied onto the substrates using a spin speed of 4000 rpm and a spin time of 30 seconds. A pre-exposure bake at 110°C for 90 seconds was performed immediately following the spin, after which the film thickness was measured at several points on the wafer surface using a Nanospec/DUV microspectrophotometer.

Large-area exposures were carried out on a system developed at UC Berkeley that uses a computer-controlled stage to step the wafer through a series of up to 15 different exposure doses, creating a matrix of exposure zones on the wafer surface for subsequent dissolution measurements. The illumination source was a Cymer KrF excimer laser with an output wavelength of 248 nm. A post-exposure bake at 110°C for 90 seconds was performed on a hotplate immediately following the exposure to reduce possible contamination effects.

Dissolution measurements were made in a tank of recirculated developer with a Perkin-Elmer development-rate monitor (DRM) that measures resist thickness by interferometry. In this way thickness vs. development time data was obtained for the entire matrix of exposure doses. The developer used was 0.18 N tetramethyl ammonium hydroxide (TMAH), achieved by mixing 2:1 H_2O:Shipley MF312 aqueous developer for SNR248 and 1:4 H_2O:Shipley MF321 aqueous developer for the four ML resists. MF321 was used to remain consistent with preliminary work done by Fréchet's group at Cornell.

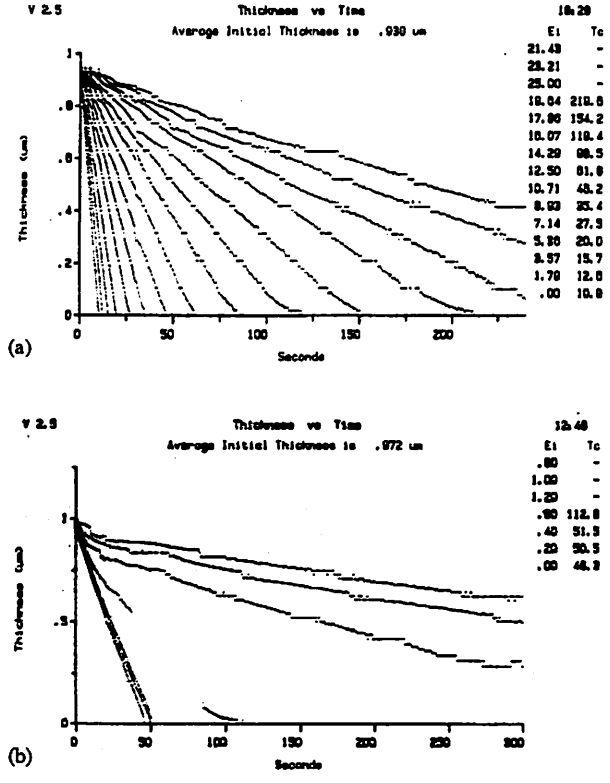

Figure 3. DRM plots of resist thickness remaining vs. development time for (a) Shipley SNR248 and (b) ML93. Data are for a matrix of exposure doses whose values are printed along the right side of the plots. The top line in each plot corresponds to the dose at which 80% of initial film thickness remains after 60 seconds.

Figure 3 contains data printed directly from the DRM with resist thickness vs. development time for SNR248 [figure 3(a)] and ML93 [figure 3(b)]. Note the very quick transition of ML93 from a very high (unexposed) development rate to the lower (exposed) development rate, as compared to the much smoother transition exhibited by SNR248. Also note what appears to be missing data for ML93 at intermediate exposure doses, which is due to nonuniform dissolution at these doses, resulting in a noisy interferometric signal and loss of thickness information.

From the data of figure 3, a graph, such as the one in figure 4(a), containing the average development rate at each exposure dose for both resists can be derived. This chart shows that

ML93 appears to be from 20 to 50 times more sensitive than SNR248, needing less than 1 mJ/cm^2 to achieve sufficient crosslinking to inhibit dissolution. It is important to mention at this point that, although actual crosslinking was not directly measured in this study, it has been shown elsewhere that true crosslinking does indeed occur at these low exposure doses.[27] The high sensitivity of ML93 is probably due at least in part to the fact that it contains an onium salt PAG.

The data in figure 4(a) is often displayed in a different format, with the resist thickness remaining at a given development time vs. exposure energy [figure 4(b)]. In order to compare ML93 and SNR248 in this format, a development time equal to 1.5 times the time to clear for unexposed regions was chosen for each resist. This formula leads to a development time of 18 seconds for SNR248 and 75 seconds for ML93. From figure 4 the contrast (γ) of each resist can be approximated. These results indicate that the γ of ML93 is roughly 2.6, while that of SNR248 is 1.4.

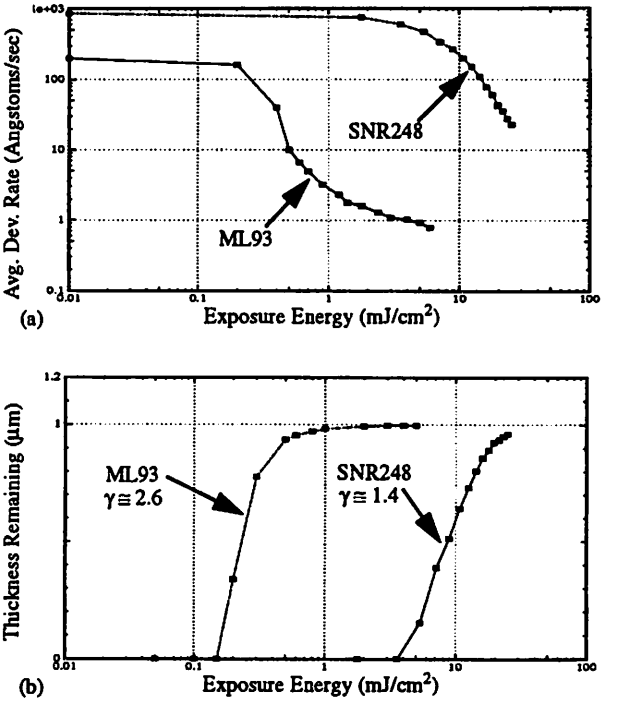

Figure 4. (a) Average development rate vs. exposure dose for ML93 and SNR248, derived from figure 3. (b) Thickness remaining vs. exposure dose after 75 seconds for ML93 and 18 seconds for SNR248. Approximate values of γ are displayed next to each curve.

Using the same process, thickness remaining vs. exposure energy curves similar to figure 4(b) were obtained comparing ML93, ML239, ML240, and ML241. These curves are plotted in figure 5. Upon comparing the dissolution curves for ML93 in figures 4(b) and 5, the careful observer may note that they appear somewhat different. Some experimental reproducibility problems have been encountered, most likely due to a combination of factors including the imaging quality of the exposure systems used and suspected airborne basic contamination in the microlab.[11]

One interesting aspect of figure 5 observed on all runs of the same experiment is that the ML239 resist appears to be about half as sensitive as ML93, ML240, and ML241. Recall that ML239 has four available crosslinking sites, while the other resists have two available sites. This lends further evidence to the idea that a greater number of available crosslinking sites on the crosslinker molecule does not increase the sensitivity of the photoresist. It has been suggested that more than two sites simply results in useless extra bonds to the same macromolecules since the bonds must be localized to the crosslinker molecule.[28] Thus once two PHOST molecules are crosslinked through two activated sites on a crosslinker molecule, activation of more sites would simply cause redundant crosslinking between the same two PHOST molecules. This leads to a decrease in sensitivity since more photoacid is required to achieve enough useful crosslinks to render the photoresist insoluble. Logically, since ML239 has twice the number of available crosslinking sites on each crosslinker molecule, it requires twice as much photoacid (and hence twice as much exposure) to achieve the same number of useful crosslinks as the other three ML resists.

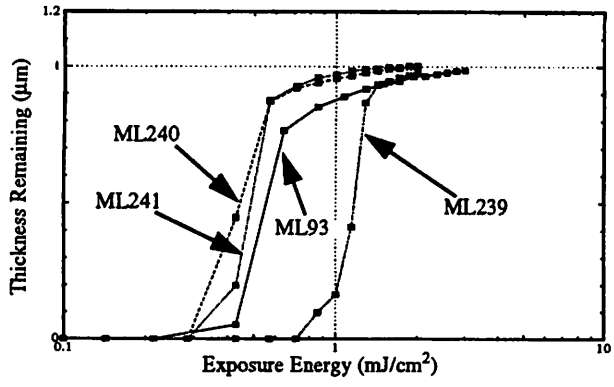

Figure 5. Thickness remaining vs. exposure dose for ML93, ML239, ML240, and ML241, in the same format as figure 4(b).

Another interesting aspect of figure 5, also observed on all runs of the same experiment, is that the dissolution rate characteristics of ML93, ML240, and ML241 are very similar. These three resists all have two sites per crosslinker molecule, but ML93 has two additional phenolic hydroxyls and ML240 has one additional phenolic hydroxyl. These extra phenolic groups were included to enhance the solubility of the resist in aqueous base, but they appear to have no effect. This suggests that the structure of the crosslinker molecule has very little effect on the dissolution process.

To assess the resolution performance of these resists, wafers were processed and examined on a scanning electron microscope (SEM). Wafer priming, resist application, and pre-exposure bake were all done using the same steps as previously outlined. Exposure was done using the Berkeley deep-UV microstepper,[29] a projection system with NA=0.6 and σ=0.5 at an exposure wavelength of 248 nm. The mask consisted of several line/space patterns of feature sizes ranging from 0.1 to 2 μm.

A matrix of different exposure doses and focal lengths was made using the deep-UV microstepper. Immediately following exposure, a post-exposure bake of 110°C for 90 seconds was done on a hotplate. Wafers were developed in the same developer tank as that used for the DRM, again using 0.18 N TMAH developer. The development time was chosen by visually observing the wafer surface as dissolution proceeded, and removing the wafers shortly after all resist was developed from the unexposed regions. Optical inspection of the line/space patterns dictated where to cleave the wafer to obtain the best SEM profile. The samples were coated with 10 nm of gold and examined in a Cwikscan SEM in the Berkeley microlab.

Four ML93 profile cross sections from the SEM are presented in figure 6. First, typical 1.0-μm [figure 6(a)] and 0.5-μm [figure 6(b)] line/space patterns are shown. While these profiles exhibit severe rounding of the corners and some bridging, they are reasonable results for a "first-pass" experiment with very little process refinement. It is speculated that the bridging seen at the base of the 0.5-μm lines may be a result of partially crosslinked PHOST molecules collapsing after uncrosslinked molecules are removed during development. The imaging quality of the microstepper is also in question,[30] which might help to explain why crosslinking occurs in the dark regions where no light is supposed to illuminate the resist. Figures 6(c) and 6(d) show two SEM cross sections of 0.4-μm features. While the lines and spaces seemed to print reasonably well, an adhesion problem was observed in that several lines either partially or completely lifted off. This is particularly well illustrated in figure 6(c). The profiles of figure 6 were exposed with 1.4 mJ/cm^2, which corresponds to over-exposure in the plots of figure 4(a) and 4(b). However, at lower exposure doses, linewidths smaller than 0.5 μm were, in general, completely lifted off. The source of this adhesion problem is unclear, but it might be due in part to the nonuniform dissolution properties discussed earlier.

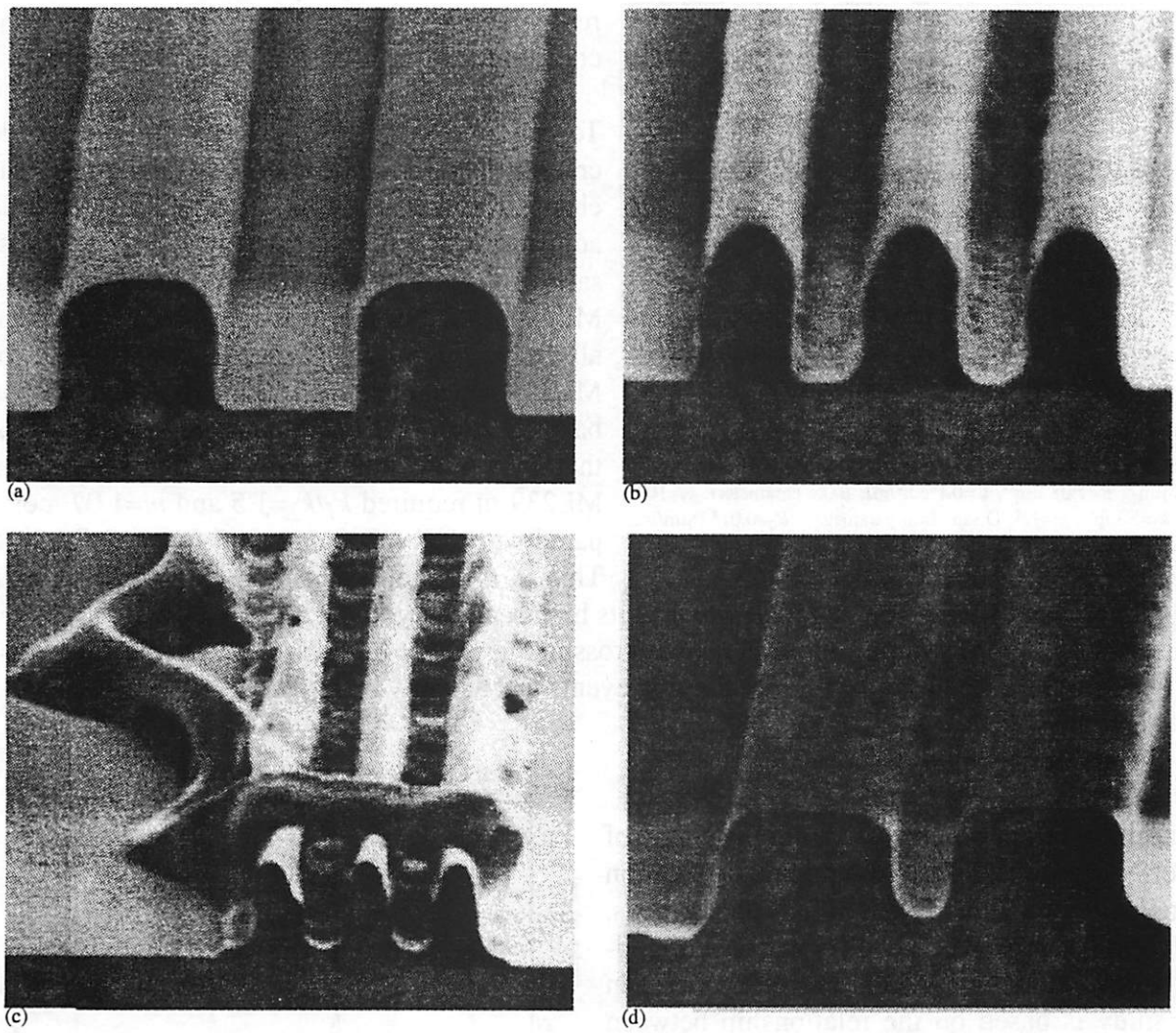

Figure 6. Scanning electron microscope (SEM) profiles of cross sections of ML93 resist: (a) 1.0-μm line/space pattern, (b) 0.5-μm line/space pattern, (c) 0.4-μm line/space pattern, and (d) 0.4-μm space between 1.5-μm lines.

3.3 Simulation

To test the validity of current resist models, an attempt was made to apply Ferguson's dissolution model for negative chemically-amplified resists[3] (described in section 2.1, equations 2.3-2.7) to the four experimental photoresists from Fréchet. Figure 7 contains an eyeball curve fit to empirical dissolution data for ML93. A reasonably good fit was made to the "knee" portion of the data. The significance of the "tail" of the empirical ML93 curve is not well understood, and is not included in any of the model equations. It is most likely due to experimental error in the data, since film thickness loss at such small dissolution rates is difficult to measure, and is insignificant anyway. The model parameters obtained from the curve fit were then used in SAMPLE, generating the profiles shown in figure 8. The most noticeable difference between the simulated profiles and the SEM cross sections of figure 6 is the rounded corners that are missing from the simulation. This might be due to contamination in the top of the resist film, as mentioned before, and also to the image quality of the Berkeley deep-UV microstepper. In addition, dissolution phenom-

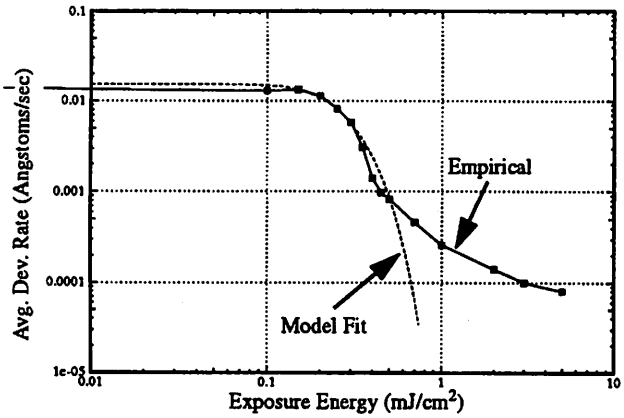

Figure 7. Curve fit of the kinetic model equations to empirical data for ML93. The parameters used in the curve fit are: Dill parameters: A=0.068 μm^{-1}, B=1.08 μm^{-1}, C=0.1 cm^2/mJ; Bake parameters: k_1=1000 sec^{-1}, k_2=5 sec^{-1}, m=1.5; Dissolution parameters: R_0=0.0153 μm/sec, C_0=4.8, α=25, n_m=5, n_s=2.

ena which occur at sharp curvature sites not currently included in SAMPLE may also need to be considered.

To model ML239, which has four available crosslinking sites, the model parameter n_s was changed from two to four. It was hoped that little adjustment to other parameters would be necessary to achieve a similar curve fit to empirical ML239 data, but this was not the case. Eventually, a curve similar to figure 7 was achieved for ML239, but at the expense of greatly varying the bake reaction-rate coefficients to such a degree that they may not make physical sense. The ML239 fit required k_1/k_2=1.5 and m=1.07, compared with k_1/k_2=200 and m=5 for the ML93 fit. This is extremely suspicious, and illustrates a basic drawback of Ferguson's model, which is its high sensitivity to n_s. As pointed out in the previous section, simply adding more available crosslinking sites to the crosslinker molecule does not increase the amount of useful crosslinking events that actually occur.

3.4 Conclusions

Several important points arise from this study of the effects of crosslinker structure on dissolution of negative chemically-amplified photoresists. First and foremost, the need for improved modelling techniques is evident. The model used in this study is based on the relationship between polymer average molecular weight and dissolution rate described by equation 2.1, and its statistical description of crosslinking is very sensitive to n_s, the number of available crosslinking sites on each crosslinker molecule. The results of experiments carried out on the four experimental resists from Fréchet suggest a very different dependence on n_s, which could be implemented by modifying equations 2.6 and 2.7. However, more important is the assumption that equation 2.1 is valid for crosslinking materials. Network polymers exhibit very different characteristics than solids of linear-chain polymers, such as very (sometimes infinitely) high melting points and swelling in compatible solvents,[17] suggesting that dissolution occurs by fundamentally different mechanisms which need to be understood

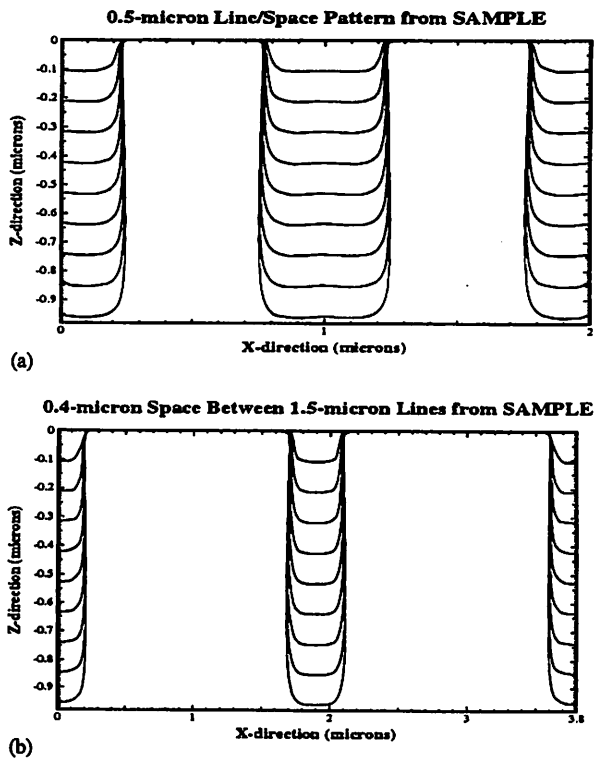

Figure 8. Profile cross sections generated by SAMPLE using the ML93 parameters from Fig. 6. Profile (a) is a 0.5-μm line/space pattern, and profile (b) is a 0.4-μm space between two 1.5-μm lines, for comparison with Figs. 5(b) and 5(d).

before a valid model can be developed.

It has been suggested that a better way to approach dissolution of crosslinking resists is with gelation theory.[31] A "gel" is defined as a non-dissolvable network polymer, and the "gel point" is defined as the threshold amount of crosslinking necessary to form a gel, or to render the polymer insoluble. Some simple gel point calculations for ML93 are presented in appendix A to determine how many crosslinking events must occur before the resist is fully exposed and to give an idea of how efficient the crosslinking process is. However, this type of theory does not describe how non-gel portions of the network dissolve, nor does it quantify the swelling observed when liquid diffuses into a gel.

It seems clear that the molecular structure of the crosslinker has very little effect on the average bulk dissolution characteristics of these resists. The next chapter presents a shift in focus from examining crosslinker structure to examining the effect of the base polymer structure on dissolution.

4.0 Polymer Dissolution Studies

The interaction of liquids with amorphous polymer solids is very complex. The physics of polymer dissolution is an area of active research in many research centers, and some progress has been made. Since resists with phenolic polymers (such as novolac and poly-hydroxystyrene) are currently the most heavily-used in industry, the first section of this chapter focuses on dissolution studies of these materials. The second section presents some molecular-level simulation ideas, and a simple chain-scission simulation program is applied to poly(methyl methacrylate) to show how simulation can be used to learn more about fundamental dissolution mechanisms.

4.1 Amphiphilic systems

Amphiphilic materials are those which display both hydrophilic ("water-loving") and hydrophobic ("water-avoiding") characteristics. Phenol molecules are a good example. Most IC lithography systems today employ photoresists with novolac base polymer. Novolac macromolecules are basically strings of phenol molecules. Poly(4-hydroxystyrene) is also phenolic. Figure 9 shows the structure of a phenol molecule. The polarity of the hydroxyl group makes it hydrophilic, and the rest of the molecule (the benzene ring) is non-polar and thus hydrophobic.

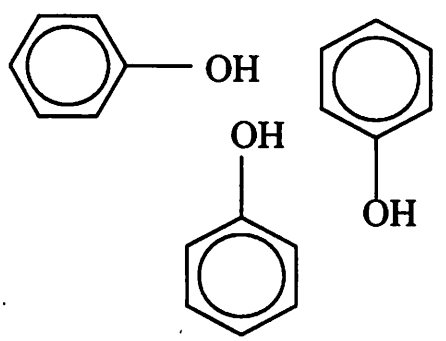

Figure 9. Structure of phenol molecules.

The basic dissolution mechanism of single phenol molecules in aqueous developer is outlined in figure 10. A solid chunk of phenol molecules placed in aqueous developer will dissolve by deprotonation of the hydroxyl.[1] First the developer molecule ROH dissociates in water to form ions R^+ (a cation radical, like K^+ or TMA^+) and OH^- (hydroxide ion). Second, the hydroxide takes a proton from the phenolic hydroxyl, leaving an extra electron with the deprotonated site (O^-). (The phenol molecule is now called a phenolate.) This extra charge is then compensated by the nearby cation R^+. At this point the phenol molecule is "dissolved". It is evident that the hydroxyl group is where all reactions take place and the

rest of the phenol molecule is unreactive. If a non-polar organic solvent is used instead of aqueous solvent, the opposite occurs - i.e. dissolution reactions take place on the benzene and the hydroxyl is unreactive. However, the advantage of using aqueous solvents is that they are much cleaner and safer, so the discussion here will be restricted to phenol dissolution in polar solvents.

This seemingly simple picture of phenol dissolution becomes very complicated for phenolic macromolecules. Since all dissolution reactions involve the hydroxyl, it is logical that the way in which the hydroxyl groups are oriented in a polymer solid is important in determining the dissolution characteristics of the polymer. Several factors need to be considered, including the connectivity, conformations, and molecular weight distribution of the polymer molecules, the way in which the developer ions diffuse through the polymer solid, and the type of radical used as the developer cation.

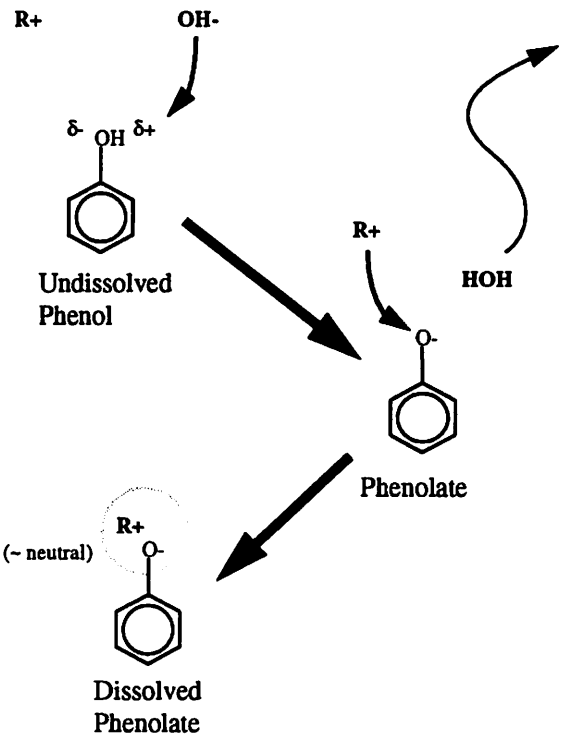

Figure 10. The three-step dissolution mechanism of phenol.

The most complete theory today to describe how developer ions move through an amphiphilic polymer matrix is percolation.[32] This theory suggests that developer base (hydroxide) ions deprotonate surface phenolic hydroxyl groups, leaving phenolate ions and loosely-bound developer cations. Base molecules then percolate along a path of available phenolate ions into the polymer solid. Each time an unreacted phenol is encountered, there is an energy barrier that must be overcome in order for deprotonation to occur, thus providing another phenolate ion for percolation to proceed. Electrostatic calculations of the interaction of a free ion (the developer base) with a dipole (the phenolic hydroxyl) can be carried out to give the energy barrier. The probability that developer will transfer between two sites separated by an energy barrier E is approximately given by a Boltzmann factor, exp(-E/RT).

In order to apply percolation theory, one must know the spatial arrangement of the OH groups in the polymer solid. This is an area of much debate, and will be discussed shortly. Currently, percolation theory has been applied to a 3D matrix containing the appropriate concentration of hydroxyls placed at random. A 2D example is shown in figure 11. The result is a scaling law of the form

$$R = B(p - p_c)^2 \qquad 4.1$$

where R is the dissolution rate, p is the fraction of phenolic hydroxyl groups in the matrix, p_c is the percolation threshold (the value of p above which dissolution occurs), and B is a constant related to the dissolution rate of some reference polymer. The reference polymer used was poly(4-hydroxystyrene) because it is the fastest dissolving phenolic polymer. Dissolution experiments on a series of novolacs with NaOH aqueous developer were carried out to test equation 4.1. The

value of p was varied by methylating a known fraction of the OH groups in several different novolac samples.

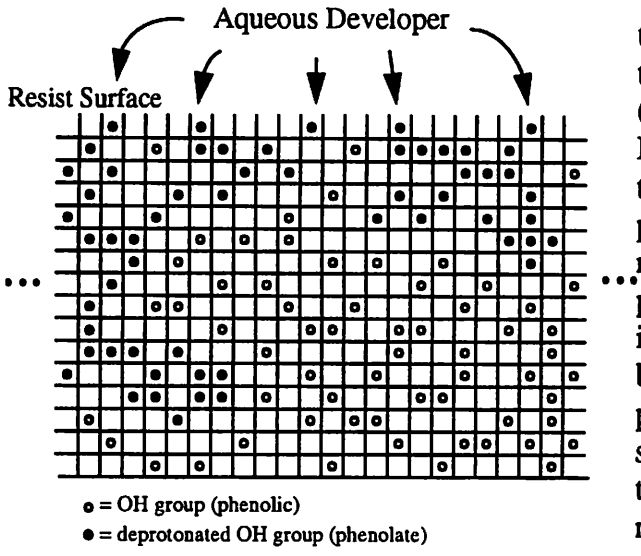

Figure 11. Example 2D percolation field. Developer base has percolated as far as possible, and the remaining phenolic hydroxyls are inaccessible due to their separation from nearest neighbors.

The results of this work appear to uphold equation 4.1 very well. Further work has been done to introduce the effects of diazonaphthoquinone (DNQ) inhibitors into the 3D percolation matrix. It is believed that DNQ works to inhibit dissolution of a novolac polymer by attracting nearby phenolic OH groups so that they become removed from the developer base percolation paths. Upon exposure, the DNQ is transformed into an indenecarboxylic acid that no longer binds the OH groups, thus releasing them to a percolation path and rendering the novolac base-soluble.[12] To apply percolation to this problem, the previous 3D random matrix is modified by randomly placing DNQ molecules in the matrix, and then adjusting the position of nearby hydroxyls to account for the attractive force of the DNQ, a 2D version of which is shown in figure 12.[33]

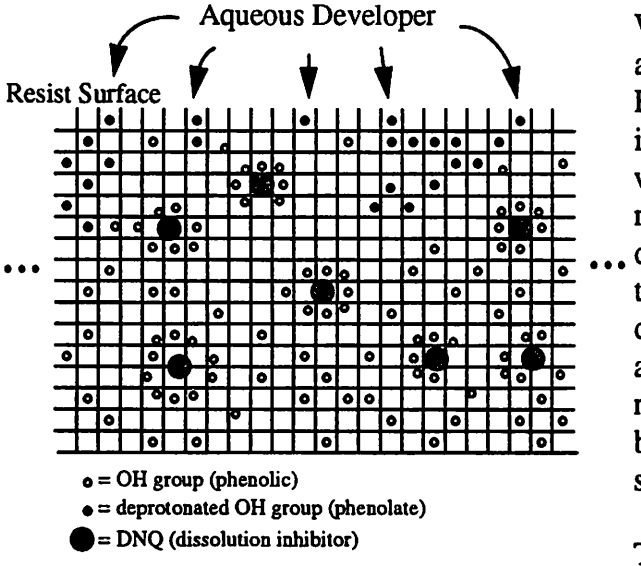

Figure 12. Example 2D percolation field in the presence on DNQ dissolution inhibitor molecules. Note that the phenolic hydroxyls tend to cluster around the DNQ molecule, thereby inhibiting percolative diffusion of developer base.

While the percolation theory of Reiser was applied with good results to dissolution in $NaOH_{(aq)}$ of polymers with regular, linear structure,[32] it has been shown that equation 4.1 does not fit well to other novolac structures (such as ortho,ortho'-coupled novolacs) dissolved in aqueous developers with different cations.[34] In particular, tetramethyl ammonium hydroxide (TMAH) developer produces very different results. There are several possible explanations that suggest modification of the basic percolation scaling law, but first a general discussion of novolac polymer structure is necessary.

The convention o[rtho], p[ara], or m[eta] describes the relative position of two substituents of an aromatic ring, as illustrated by figure 13. Thus an ortho,ortho'-coupled novolac is a polymer formed by connecting phenol monomers in an "ortho,ortho'" configuration with respect to the OH group [shown in figure 14(a)]. It is important to note that novolacs always have aromatic rings in the polymer backbone. In the case of poly(4-hydroxystyrene), shown in figure 14(b), the polymer backbone is carbon, and the aromatic rings are contained in the side groups.

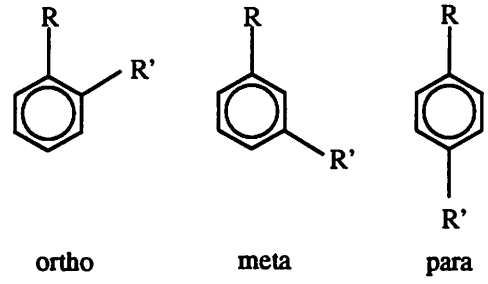

Figure 13. Convention in describing the relative position of two substituents of an aromatic ring.

The type of connectivity of novolac monomers greatly affects the conformational shape of the resulting macromolecules. Molecular mechanics simulations show that different types of novolacs exhibit different molecular conformations based on the proximity of nearest-neighbor hydroxyl groups.[35] Since an OH group is polar, it is attracted to nearby OH groups by hydrogen bonding, tending to pull them close if possible. Thus if several hydroxyl groups on a particular macromolecule are in close proximity, they will be attracted to each other (*intra*molecular hydrogen bonds) and cause the molecule to "curl up". The extreme case for intramolecular hydrogen bonding is ortho,ortho'-coupled novolac, shown in figure 14(a). Conversely, if a given OH group's nearest neighbor hydroxyls belong to different macromolecules, *inter*molecular bonding will be favored and the molecules will tend to "stretch out". The extreme case for intermolecular bonding is polyhydroxystyrene [figure 14(b)].

In addition, the rigidity of the backbone and steric hindrances of large side groups also play important roles in determining molecular shape.[24] Often hydrogen bonding and bond-angle stretching are opposing forces (as with ortho,ortho'-coupled novolac - the aromatic ring in the backbone makes the macromolecule very rigid, but hydrogen bonds put stress on the macromolecule to curl up), making it difficult to determine the conformation of lowest energy.

These concerns regarding the shape of the novolac molecules help determine the spatial distribution of OH groups in a percolation field. Polymers with a high degree of intermolecular hydrogen bonding (such as PHOST and ortho,-para'-coupled novolac) most likely give a nearly randomly-oriented percolation field, providing many percolation paths and dissolving quickly. But polymers with more intramolecular bonding (such as ortho,ortho'-coupled novolac) probably exhibit a more "clustered" percolation field, with many isolated groups of hydroxyls. These isolated groups would greatly decrease the number of percolation paths available to developer base, and thus the overall dissolution rate of these polymers would be much slower. This is indeed the case.[35]

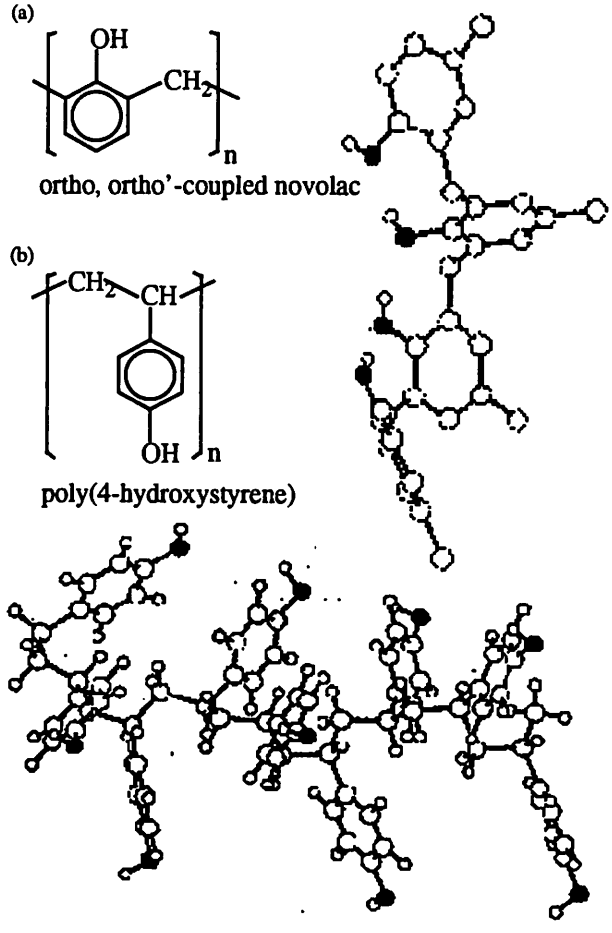

Figure 14. Structure and molecular mechanics simulation of (a) ortho,ortho'-coupled novolac and (b) poly(4-hydroxystyrene). Note the "spiral" shape of PHOST compared with the "cluster" of the novolac hydroxyls.[35]

Other factors that place the scaling law of equation 4.1 in question are the effects of the size of the developer cation and the possible existence of diffusion modes other than percolation. Once an OH group is deprotonated, there is an extra electron that can move about for some amount of time before the developer cation can move in and bind it. Taking a closer look [figure 15], it seems reasonable that if several hydroxyl groups are in close proximity and one of the sites is deprotonated, the liberated electron could become delocalized and move from one hydroxyl site to another.[36] The presence of this extra charge repelling developer base ions would make subsequent deprotonations much more difficult (by greatly increasing the energy barrier for percolative site transfer).

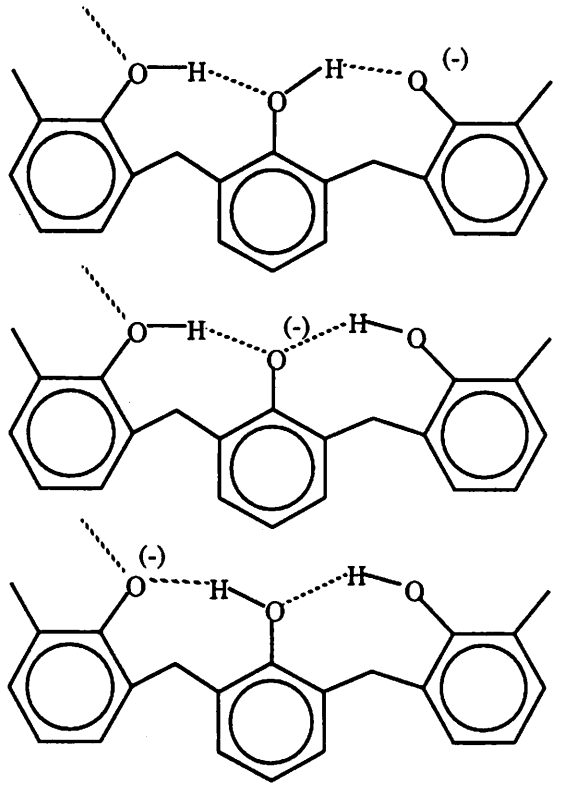

Figure 15. Illustration of electron delocalization in a cluster of hydrogen-bonded phenolic hydroxyl groups.[36]

The degree to which this can happen is based on at least two factors: first, the distance between OH groups, determined by the novolac conformational structure, and second, the ability of the developer cation to quickly neutralize the free charge. The second factor presumably depends on the physical size of the cation, its electronegativity, and the amount of space available for the cation to move about in. Thus a large cation like TMA^+ would not be able to move around as freely as a smaller cation like K^+ or Na^+, resulting in much looser binding of the extra electron, in turn making deprotonation more difficult and slowing dissolution.

Developer diffusion modes other than percolation may also exist in phenolic polymers.[34] Any free volume would allow very fast penetration of solvent. Indeed, it has been suggested that the dissolution acceleration properties of exposed DNQ inhibitor molecules (which have been transformed into indenecarboxylic acids) are a result of the photolytic evolution of nitrogen during the exposure reaction, which causes an increase in free volume in the resist.[12]

Thus it is clear that the general percolation scaling law (equation 4.1) does not include all potential dissolution phenomena, and may have to be modified in some circumstances where these other phenomena are important. Reiser's experiments used novolacs whose phenolic hydroxyl groups participate mainly in *inter*molecular hydrogen bonding, leading to a nearly random spatial distribution. They also used $NaOH_{(aq)}$ developer, which has a small cation that can better localize the phenolate negative charge to facilitate deprotonation of nearby hydroxyl groups. Experiments with other resists using $TMAH_{(aq)}$ developer support the percolation law, but with an exponent other than two.[34]

To date, percolation has been applied only to a matrix of hydroxyl sites oriented at random in

space. No information about their connectivity has been implemented, and there is mounting evidence that the polymer molecular weight distribution also plays an important role in determining the dissolution characteristics of photoresists. The next section examines some possible effects of molecular weight distributions, and presents the results of a simple chain-scission simulation program that raise some interesting questions about the weight distribution of one-component positive resists before and after exposure.

4.2 Molecular weight simulations

With percolation theory making progress in describing how developer base diffuses into an amphiphilic polymer, there are many questions regarding how polymer molecular weight distribution affects the removal of sufficiently deprotonated polymer chains. More generally, the relationship between the distribution of macromolecular sizes in any organic resist film and its dissolution characteristics has yet to be fully determined. The molecular weight models based on equation 2.1 relate dissolution rate to *average* molecular weight, but there is evidence that dissolution is also dependent on the *distribution* of molecular weight. It has been suggested that polymers with small polydispersity follow equation 2.1, but those with larger polydispersity dissolve at a rate dictated by the lower molecular-weight portions of the polymer.[37] One possible explanation for this behavior is the "stone wall" model (illustrated in figure 16), suggesting that while larger molecules take more time to dissolve, the presence of many small, quickly developing molecules may open up free volume around the larger molecules to enhance their dissolution.[38]

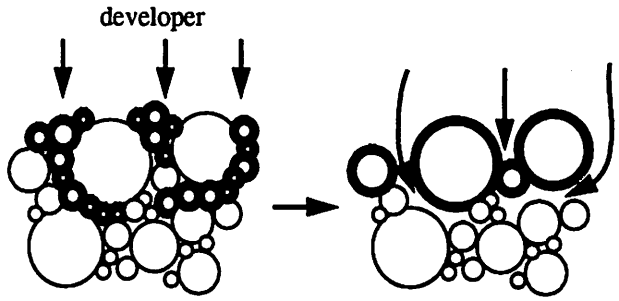

Figure 16. Illustration of the "stone wall" model of dissolution of a polydisperse polymer. Molecules of low molecular weight dissolve quickly, creating free volume for developer to penetrate the polymer matrix and carry away high molecular weight molecules, resulting in a much higher dissolution rate than predicted by the average molecular weight of the polymer.

Experimental work is currently being done to clarify the many uncertainties about how macromolecular size distribution influences dissolution.[37, 39] Simulation can also be used as a tool for discerning some of these uncertainties. Any molecular-level photoresist dissolution simulator must certainly contain information about the molecular weight distribution of the base polymer. To this end, a simple simulation program for one-component chain-scission photoresists has been written that reads a user-defined distribution of polymerization and performs a given number of chain-scission events. The program outputs the resulting polymerization distribution.

Photo-initiated bond breaking is the mechanism by which one-component resists become soluble. Thus the simulation program keeps track of monomer-monomer bonds. Each macromolecule to be simulated is assigned a reference number. The program maintains a linked list data structure with each node representing a bond and containing the reference to the macromolecule it belongs to. For each scission event, a bond is chosen at random and the corresponding node is removed from the linked list. A new macromolecule is added by updating the reference number of all nodes following the removed node belonging to the molecule that was cut. Thus for each scission, the number of nodes (or monomer-monomer bonds) decreases by one, and the number of macromol-

ecules in the system increases by one.

The bond linked list is created from an input file containing the distribution of polymerization as defined by the user. Specifically, each line in the file represents one macromolecule, and the number given is the degree of polymerization of that molecule. The simulation program reads this file as follows: the number d_1 from the first line is scanned. Since d_1 is the number of monomers comprising the first macromolecule, the number of bonds is simply d_1-1. Thus d_1-1 nodes are added to the (initially empty) linked list. Each node is given a reference number 1, corresponding to the first macromolecule input. Then the number d_2 is read from the second line, and d_2-1 nodes are added to the list with each node assigned reference number 2, and so forth.

Once the bond list is completed, the user is prompted for the number of scission events to occur. After performing the required action, the resulting linked list is written to an output file in the reverse of the input steps, leaving a table of the number of macromolecules that have each degree of polymerization. The C program code is provided in appendix B.

As an example, electron-beam exposure of a poly(methyl methacrylate), or PMMA, was simulated. The number-averaged molecular weight of PMMA is typically 600000, which is equal to degree of polymerization of 6000 (the molecular weight of methyl methacrylate is 100 grams/mol). Typical exposure doses needed to significantly increase the solubility of PMMA are around 75 $\mu C/cm^2$ at 20 keV, which corresponds to about 1.2×10^{22} eV/cm^3 of energy deposited in the resist. The scission efficiency (called G(s) in literature[12]) is 0.013 scissions/eV. Straightforward algebraic calculations (using the density of PMMA, which is ρ=1.275 grams/cm^3) show that at this dose, about two percent of the bonds available for scission are actually cut.

Thirty molecules with degree of polymerization of 6000 were given as input to the simulation program, resulting in a linked list of 5999x30 ≅ 180000 bonds. Scission of two percent of these bonds means 3600 scission events must be simulated. Figure 17(a) shows the polymerization distribution after half of this exposure (1800 scission events), and results of the full dose are shown in figure 17(b). To convert degree of polymerization into molecular weight, one needs only to

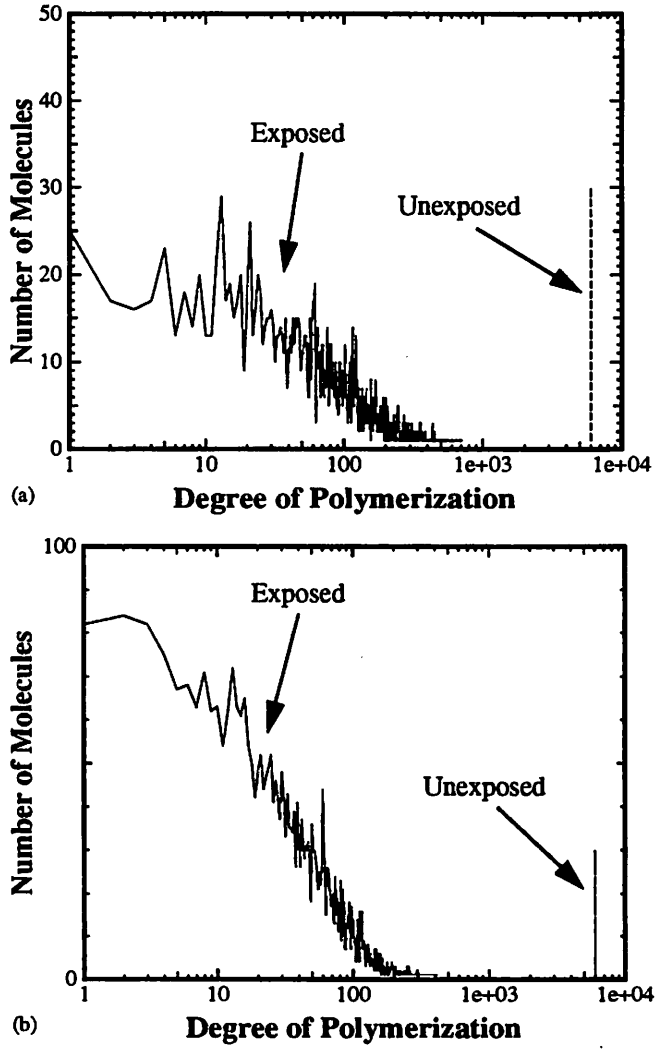

Figure 17. Chain scission simulation results of PMMA after (a) half exposure and (b) full exposure.

multiply by the molar mass of a PMMA monomer (which is 100 grams/mol).

It is clear from figure 17 that the average molecular weight quickly decreases during exposure. This simple program does not actually predict the dissolution characteristics of the resulting polymer mass distribution, but results such as this can be used in conjunction with experiment to get an idea of how dissolution proceeds on a molecular level. For instance, these simulations show that a very narrowly-polydisperse sample undergoing chain scission rapidly breaks up into a sample with a very wide distribution of polymerization. In order to achieve sufficiently high dissolution rates to be considered fully exposed, it is apparent from figure 17(b) that the PMMA sample consists mostly of small molecules, with very few of them containing over 100 monomers. While it is not clear from the simulations whether the polydispersity of an exposed sample plays a role in the resulting dissolution speed, these results can be used in conjunction with dissolution experiments on low molecular-weight samples of varying polydispersity to provide more information.

5.0 Conclusions and Directions for Future Work

Current IC process simulation packages have enjoyed reasonable success in predicting the response of well characterized lithography systems. Empirical photoresist models such as those discussed in chapter 2 can be easily constructed to relate the average dissolution rate to exposure dose, which can then be implemented into etch-front simulators such as SAMPLE or PROLITH. However, as IC feature dimensions continue to shrink, the finite size of resist macromolecules is becoming more of an issue. Empirical etch-front models do not reveal molecular-scale effects, and provide little help in designing new resist systems necessary for manufacturing use at higher frequency exposure radiation.

Increased understanding and improvement in modelling techniques of photoresist dissolution mechanisms must occur in order to understand and quantify molecular-scale effects (such as surface roughness of resist features) that are increasingly significant in the IC industry, and to aid in future resist synthesis applications. Obviously physical understanding must first be gained before appropriate simulators can be developed. However, theoretical simulations can greatly facilitate the approach of physical understanding by providing the ability to test any mechanism of choice to see if that mechanism explains experimental results.

Experimental work is being done to assess dissolution mechanisms. In chapter 3 of this paper, crosslinker studies in negative three-component resists revealed that varying the structure of the crosslinker molecule has little effect on dissolution characteristics, other than a decrease in sensitivity with a corresponding increase in the number of available crosslinking sites. Other work by different research groups continues to unravel the complicated physics of dissolution in two-component novolac resists.

As shown by the one-component positive resist simulations of section 4.2, much can be learned with simulation about the distribution of molecular weight in a resist at various exposure doses. Combined with experimental data providing the dissolution rate at these doses, a more complete view of dissolution mechanisms can be obtained. In addition, as mentioned above, experiments on low average molecular-weight samples of varying polydispersity would also be very useful in further quantizing how molecular weight distribution affects the dissolution characteristics.

It is precisely this type of work that is currently being done with novolacs.[37,39] Although novolac-based photoresists do not undergo molecular weight changes to achieve developer selectivity, the distribution of molecular sizes still appears to have significant effects on dissolution. A quantitative understanding of these effects and their physical mechanisms will provide another lever with which to optimize novolac resist performance.

With progress being made in theories of diffusion of developer base into amphiphilic polymer solids, and experimental work being carried out to understand molecular size effects, it seems that an appropriate simulation tool for novolac polymers would be very beneficial. Since it is likely that most of the dissolution chemistry occurs at the phenolic hydroxyl groups, perhaps a data structure such as that used to keep track of bonds in the one-component positive resist simulation program of chapter 4.2 could be used to keep track of phenolic hydroxyl groups and phenolate sites in a novolac simulation program. Each node would represent an OH group, and would contain a reference number for the macromolecule it belongs to and coordinates of its spatial position. Diffusion mechanisms such as percolation could then be applied, with the state of a node being changed form phenolic to phenolate as deprotonation occurs.

There are several hurdles to overcome in designing such a simulator. The most prominent is the method of determining the spatial arrangement of OH groups. Presumably one macromolecule at a time would be set up, using molecular mechanics to determine its conformations and measured density to determine intermolecular spacing, and then the positions of the OH groups would be read from that. It has been shown that in a pure amorphous polymer the macromolecules adopt their unperturbed dimensions,[17] so presumably this guideline can be used to provide the macromolecular shape in the solid photoresist. Another hurdle is keeping track of extra charges liberated by deprotonation. Presumably movement of these charges can be modelled with an electrostatic approach similar to that used in modelling the interaction of the (charged) developer base and the dipole OH groups. Yet another hurdle is in determining how many deprotonations must occur on a given macromolecule before it is released from the solid state and carried away by the aqueous developer.

Obviously such a simulation program would become complicated very quickly. It also necessarily must make many assumptions about the underlying physics, but these assumptions are exactly what such a model would be designed to test. As physical understanding of dissolution mechanisms grows, the initial assumptions would be continually updated, and new theories could be implemented to compare to experimental data. From engineering and manufacturing viewpoints, this rigorous approach may not seem necessary. However, macroscopic approaches to resist simulation will no longer be adequate as feature dimensions become on the order of macromolecular dimensions. It is clear that photoresist materials and modelling techniques will have to be improved in many ways to keep up with increasing lithographic demands of the IC industry.

6.0 Acknowledgments

Thanks to my advisor Prof. A. R. Neureuther for a great couple of years, and for his words of encouragement. Additional thanks to Prof. W. G. Oldham and Dr. Paul Hagouel for taking time to read this report, and also to Paul and Marco Zuniga for their insightful observations and inputs.

Thanks to Kim Chan and Maria Perez for their help in the lab. Finally, thanks to Bernice Lum for all the coffeeshop discussions!

7.0 References

1. R. Dammel, *Diazonaphthoquinone-based Resists*, SPIE Optical Engineering Press **1993**.

2. F. Dill, W. Hornberger, P. Hauge, and J. Shaw, *IEEE Trans. on Electron. Devices*, vol. ED-22, no. 7 (**1975**), p. 445.

3. R. Ferguson, *Ph.D. thesis*, University of California at Berkeley, **1991**.

4. M. Zuniga, G. Wallraff, E. Tomacruz, B. Smith, C. Larson, W. Hinsburg, and A. Neureuther, *J. Vac. Sci. Technol. B*, vol. 11, no. 6 (**1993**), p. 2862.

5. P. Hagouel, *Ph.D. thesis*, University of California at Berkeley, **1976**.

6. N. Tam, *Ph.D. thesis*, University of California at Berkeley, **1991**.

7. M. O'Toole and W. Grande, *IEEE Trans. on Electron. Devices*, vol. EDL-2, no. 12 (**1981**), p. 445.

8. M. Exterkamp, W. Wong, H. Damar, A. Neureuther, C. Ting, and W. Oldham, *Proc. SPIE*, vol. 334 (**1982**), p. 182.

9. W. Bell II, P. Flanner III, C. Zee, N. Tam, and A. Neureuther, *Proc. SPIE*, vol. 920 (**1988**), p. 382.

10. D. Kim, W. Oldham, and A. Neureuther, *IEEE Trans. on Electron. Devices*, vol. ED-31, no. 2 (**1984**), p. 1730.

11. W. Hinsberg, S. MacDonald, N. Clecak, and C. Snyder, *Proc. SPIE*, vol. 1672 (**1992**).

12. C. Willson, *Introduction to Microlithography, second edition*, ed. L. Thompson, C. Willson, and M. Bowden, American Chemical Society **1994**, p. 139.

13. A. Novembre, L. Kowalski, J. Frakoviak, D. Mixon, and L. Thompson, *Solid State Technol.*, vol. 31, no. 4 (**1988**), p. 135.

14. M. Bowden, *Materials for Microlithography - ACS Symposium Series 266*, ed. L. Thompson, C. Willson, and J. Fréchet, American Chemical Society **1984**, p. 71.

15. J. O'Donnell, N. Rahman, C. Smith, and D. Winzor, *Macromolecules*, vol. 12, no. 1 (**1979**), p. 113.

16. E. Scheckler, T. Ogawa, S. Shukuri, and E. Takeda, *IEICE Trans. Electron.*, vol. E77-C, no. 2 (**1994**), p. 98.

17. R. Young and P. Lovell, *Introduction to Polymers, second ed.*, Chapman & Hall **1991**.

18. E. Scheckler, T. Ogawa, H. Yamanashi, T. Soga, et. al., *Proc. 1994 VLSI Technol. Symposium* (**1994**), p. 139.

19. T. Everhart, *Materials for Microlithography - ACS Symposium Series 266*, ed. L. Thompson, C. Willson, and J. Fréchet, American Chemical Society **1984**, p. 5.

20 H. Smith, *J. Vac. Sci. Technol. B*, vol. 4, no. 1 (**1986**), p. 148.

21. A. Neureuther and C. Willson, *J. Vac. Sci. Technol. B*, vol. 6, no. 1 (**1988**), p. 167.

22. K. Early, D. Tennant, D. Jeon, P. Mulgrew, A. MacDowell, and O. Wood II, *J. Vac. Sci. Technol. B*, vol. 10, no. 6 (**1992**), p. 2600.

23. B. Lum, *Master's thesis*, University of California at Berkeley, **1994**.

24. T. Yoshimura, H. Shiraishi, J. Yamamoto, and S. Okazaki, *Jpn. J. Appl. Phys. Part 1*, vol. 32, no. 12B (**1993**), p. 6065.

25. J. Thackeray, G. Orsula, E. Pavelchek, D. Canistro, L. Bogan, A. Berry, and K. Graziano, *Proc. SPIE*, vol. 1086 (**1989**), p. 34.

26. J. Fréchet and S. Lee, *Proc. SPIE*, vol. 1925 (**1993**), p. 102.

27. S. Lee, J. Fréchet, and C. Willson, *Macromolecules* (in press).

28. P. Trefonas and M. Allen, *Proc. SPIE*, vol. 1672 (**1992**), p. 74.

29. C. Spence, W. Oldham, W. Partlo, J. Bruning, D. Markle, and R. Hsu, *Proc. SPIE*, vol. 1088 (**1989**), p. 471.

30. C. Spence, R. Ferguson, M. Yeung, S. Das, J. Hutchinson, and A. Neureuther, *J. Vac. Sci. Technol. B*, vol. 8, no. 6 (**1990**), p. 1735.

31. A. Reiser, *Photoreactive Polymers: the Science and Technology of Resists*, John Wiley & Sons, **1989**.

32. T. Yeh, H. Shih, and A. Reiser, *Proc. SPIE*, vol. 1672 (**1992**), p. 204.

33. H. Shih, A. Reiser, *Proc. SPIE*, vol. 2438 (**1995**, in press).

34. P. Trefonas, G. Vizvary, J. Root, C. Meister, and C. Szmanda, *Proc. SPIE*, vol. 2195 (**1994**), p. 707.

35. M. Templeton, C. Szmanda, and A. Zampini, *Proc. SPIE*, vol. 771 (**1987**), p. 136.

36. C. Garza and C. Szmanda, *Proc. SPIE*, vol. 920 (**1988**), p. 321.

37. H. Shiraishi, T. Yoshimura, T. Sakamizu, T. Ueno, and S. Okazaki, *J. Vac. Sci. Technol. B*, vol. 12, no. 6 (**1994**), p. 3895.

38. M. Hanabata, Y. Uetani, and A. Furuta, *Proc. SPIE*, vol. 920 (**1988**), p. 349.

39. P. Tsiartas, L. Simpson, C. Willson, R. Allen, V. Krukonis, and P. Gallagher-Wetmore, *Proc. SPIE*, vol. 2438 (**1995**, in press).

Appendix A. Gel Point Calculations for ML93

The following is a calculation of the gel-point crosslinking density necessary to render ML93 resist insoluble. This threshold density is compared with theoretical maximum number of crosslinking events possible to give an estimate of the crosslinking efficiency. The gel point is defined as when gel (or non-dissolvable network polymer) makes its first appearance in a polymer solid. These calculations are based on Stockmayer's Rule,[31] which states that at the gel point, every macromolecule has an average of one crosslink. This leads to the following expression for the gel-point crosslink density:

$$\rho_G = \frac{M_0}{M_W} \qquad \text{A.1}$$

where M_0 is the monomer molar mass, and M_W is the weight-averaged polymer molecular weight.

The following are approximate calculations of ρ_G for ML93 negative chemically-amplified resist.

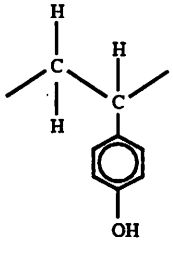

poly(4-hydroxystyrene)
19.6 wt.%

8(C)+9(H)+1(O) =>
M_0=8(12)+8(1)+16=120 g/mol

Typical mass distribution values:
$\overline{M}_n$=3900, $\overline{M}_w$=10200.

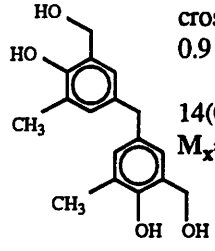

crosslinker
0.9 wt.%

14(C)+14(H)+7(O) =>
M_x=14(12)+14(1)+7(16)=294 g/mol

Thus in 1000g of resist:

The number of PHOST monomers is 0.196(1000g)(mol PHOST/120g) = 1.633 mol PHOST monomer.
Each monomer can contribute half of a crosslink
=> total possible number of crosslinks = 0.8165 mol

Using Stockmayer's rule: $\rho_G = M_0/M_w = 120/10200 = 0.0118$
=> to reach the gel point, 1.18% of the total number of possible crosslinks must have actually participated in a crosslinking event.
=> 0.0118(0.8165 mol) = **0.0096 mol crosslinking events needed to reach polymer gel point.**

The number of crosslinker molecules is 0.009(1000g)(mol crosslinker/294g) = 0.0306 mol crosslinker.
Each crosslinker can contribute one crosslinking event.
=> **total number of available crosslinking events = 0.0306 mol**

Thus the crosslinking efficiency must be (number of crosslinking events needed to reach gel point)/(total number of available crosslinks) = 0.0096/0.0306 = 0.314, or about 30% of the available crosslinking sites must be activated and participate in a crosslinking event to render ML93 insoluble based on the application of Stockmayer's rule.

Appendix B. C Code for Chain-Scission Simulation

The following is the code for the program to simulate chain scission. The results of some example runs are presented in section 4.2.

```
/* this program fills the text file "infoin" with the degree of polymerization of each molecule to be exposed.
    (compile by typing "cc fillin.c -lm") */

#include <stdio.h>
#include <stdlib.h>
#include <math.h>

main()
    {
    Fill();
    }

/* function to fill the info file */
Fill(void)
    {
    FILE *fp;
    int dop,nm,j;
    fp=fopen("infoin","w");
    nm=1;
    while(nm!=0)
                {
                printf("How many molecules (0 to stop)? -> ");
                scanf("%d",&nm);
                if(nm==0)
                                break;
                printf("Enter the degree of polymerization -> ");
                scanf("%d",&dop);
                fprintf(fp,"%d\n%d\n",(dop-1),(dop+1));
                for(j=1;j<=nm;j++)
                                fprintf(fp,"%d\n",dop);
                }
    fclose(fp);
    return;
    }

/* this program takes a given molecular weight distribution and performs a set amount of exposure events
    to determine the resulting molecular weight distribution.  All monomer-monomer bonds have equal
    probability of being cut. */

#include <stdio.h>
#include <stdlib.h>

struct node
                {
```

```
                int chain;
                struct node *next;
                };
struct node *talloc(void);

main()
    {
    struct node *firstNode,*lastNode,*currentNode;
    int NumBonds,NumMol,j,rint,NumEvents;
    double rnum;
    firstNode=NULL;
    lastNode=NULL;
    NumBonds=0;
    NumMol=0;
    FillBonds(&NumBonds,&NumMol,&firstNode,&lastNode);
    GraphOut(NumMol,firstNode);
    printf("How many scissions do you want? -> ");
    scanf("%d",&NumEvents);
    for(j=1;j<=NumEvents;j++)
                {
                rnum=(NumBonds*(1.0*rand())/RAND_MAX)+0.5;
                rint=(int)rnum;
                Event(&NumBonds,&NumMol,rint,firstNode,lastNode);
                }
    GraphOut(NumMol,firstNode);
    exit(0);
    }

/* function to fill the linked-list of bonds with data from the input file "infoin" */
FillBonds(nb,nm,first,last)
    int *nb,*nm;                                        /* nb = #bonds, nm = #molecules */
    struct node *first,*last;
    {
    FILE *fp;
    struct node *current;
    int DegreeOfPol,j;
    fp=fopen("infoin","r");                             /* open data file with molecule info */
    *nm=0;
    *nb=0;
    while((fscanf(fp,"%d\n",&DegreeOfPol))!=EOF)
                {
                ++(*nm);
                for(j=1;j<DegreeOfPol;j++)
                                {
                                ++(*nb);                /* increment the number of bonds */
                                current=talloc();       /* reserve memory for new node */
                                current->chain=(*nm);   /* label current node's molecule # */
                                current->next=NULL;
                                if(first==NULL)
                                                first=current;
```

```
                        else
                                last->next=current;
                        last=current;
                        }
                }
        fclose(fp);
        return;
        }

/* function to remove a node and update the following nodes for an exposure event */
Event(nb,nm,bond,first,last)
        int *nb,*nm,bond;                       /* bond = the bond to be cut */
        struct node *first,*last;
        {
        struct node *previous,*select,*current; /* select points to node to be cut, previous
                                                   points to node before it */
        int j,mol;                              /* mol = the current molecule */
        previous=first;
        select=first;
        if(bond==1)                             /* if the bond to be cut is the first one... */
                {
                first=first->next;              /* move the first node to the next one */
                previous=NULL;                  /* the original first node is now null */
                }
        else
                {
                for(j=2;j<bond;j++)             /* move to node before node to be cut */
                        previous=previous->next;
                select=previous->next;          /* position select at the node to be cut */
                previous->next=select->next;    /* pointer from previous node skips over
                                                   the node to be cut */
                mol=previous->chain;
                current=previous->next;
                while((current!=NULL)&&(current->chain==mol))
                        {                       /* while on this same molecule */
                        current->chain=(*nm)+1; /* make a new molecule */
                        current=current->next;
                        }
                }
        if(previous->next==last)                /* move the position of last node */
                {
                last=previous;
                last->next=NULL;
                }
        ++(*nm);                                /* increment the number of molecules */
        --(*nb);                                /* decrement the number of bonds */
        return;
        }
```

```
/* function to allocate memory for a new node */
struct node *talloc(void)
    {
    return(struct node *) malloc(sizeof(struct node));
    }

/* function to fill output file with drawplot-format data. x=degree of polymerization, y=#molecules */
GraphOut(nm,first)
    int nm;                                          /* nm = #molecules */
    struct node *first;
    {
    FILE *fp;
    struct node *current;
    int mol,MolsDone,*data,dop,j,NumPts;     /* mol=the current molecule, MolsDone=#molecules
        done, data=array of graph data, dop=degree of polymerization of mol, NumPts = #plot points */
    data=(int *) calloc(10000,sizeof(int));          /* get array space */
    for(j=0;j<10000;j++)                             /* initialize the array to zero */
            *(data+j)=0;
    fp=fopen("dataout","a");
    MolsDone=0;
    NumPts=0;
    current=first;                                   /* start at the beginning of the list */
    while(current!=NULL)
            {
            ++MolsDone;                              /* increment #molecules done */
            dop=0;                                   /* init degree of polym of ea. molecule */
            mol=current->chain;                      /* read chain # of current molecule */
            while((current!=NULL)&&(current->chain==mol))
                    {                                /* while on this same molecule */
                    ++dop;                           /* increment degree of polymerization */
                    current=current->next;
                    }
            ++(*(data+dop));                         /* increment #molecules with dop */
            }
    *data=(nm-MolsDone);                             /* fill in zero element with #monomers */
    for(j=1;j<=10000;j++)                            /* get number of points to be graphed */
            {
            if((*(data+j-1))!=0)
                    ++NumPts;
            }
    fprintf(fp,"%d\n",NumPts);                       /* write #points to drawplot file */
    for(j=1;j<=10000;j++)                            /* write to graph file */
            {
            if((*(data+j-1))!=0)                     /* write only non-zero values */
                    fprintf(fp,"%d   %d\n",j,*(data+j-1));
            }
    fclose(fp);
    return;
    }
```